

# Soft Matter

Accepted Manuscript



This is an *Accepted Manuscript*, which has been through the Royal Society of Chemistry peer review process and has been accepted for publication.

*Accepted Manuscripts* are published online shortly after acceptance, before technical editing, formatting and proof reading. Using this free service, authors can make their results available to the community, in citable form, before we publish the edited article. We will replace this *Accepted Manuscript* with the edited and formatted *Advance Article* as soon as it is available.

You can find more information about *Accepted Manuscripts* in the [Information for Authors](#).

Please note that technical editing may introduce minor changes to the text and/or graphics, which may alter content. The journal's standard [Terms & Conditions](#) and the [Ethical guidelines](#) still apply. In no event shall the Royal Society of Chemistry be held responsible for any errors or omissions in this *Accepted Manuscript* or any consequences arising from the use of any information it contains.

# Fingering patterns during droplet impact on heated surfaces

Mohammad Khavari,<sup>a,b</sup> Chao Sun,<sup>c</sup> Detlef Lohse,<sup>c</sup> and Tuan Tran<sup>\*a</sup>

Received Xth XXXXXXXXXXXX 20XX, Accepted Xth XXXXXXXXXXXX 20XX

First published on the web Xth XXXXXXXXXXXX 200X

DOI: 10.1039/b000000x

A droplet impinging on a sufficiently heated surface may be cushioned by its own vapor and never touches the surface. In prior work, the transition to this so-called Leidenfrost regime was only qualitatively described as an abrupt change between the “contact-boiling” regime, which is characterized by violent boiling behaviors, and the Leidenfrost state. We reveal that the wetted area can be used as a quantity that *quantitatively* characterizes this transition and it is a continuous function of surface temperature up to the Leidenfrost regime. The wetted area exhibits fingering patterns caused by vapor flow under the liquid. This underlines the crucial role of vapor transport in the Leidenfrost transition and unveils the physical mechanism of the transition to the Leidenfrost regime.

Boiling of an impacting droplet on a heated surface is a process that occurs when the surface temperature is sufficiently high to nucleate vapor bubbles at the solid-liquid interface during the spreading of the droplet. This process is at the heart of various technical applications such as fuel injection in combustion engines and spray cooling technologies<sup>1</sup>. One of the key targets in these applications is to control the heat flux from the surface through the boiling process. Numerous studies therefore have been motivated to obtain insight into the phenomena during the interaction between heated surfaces and a single droplet<sup>2</sup>. However, a physical understanding of the boiling process during impact is still elusive and calls for investigations of the different boiling regimes<sup>3–5</sup>, the transition between these regimes<sup>1,6</sup>, and the dependence of the heat flux on the involving physical parameters<sup>7–9</sup>.

Generally, the heat flux is a non-monotonic function of the surface temperature and the wetted area. Its minimum value occurs at the so-called Leidenfrost transition<sup>10,11</sup>, which separates two major boiling regimes: the contact boiling regime in which heat is transferred directly to the liquid, and the Leidenfrost regime in which heat is transferred through a vapor

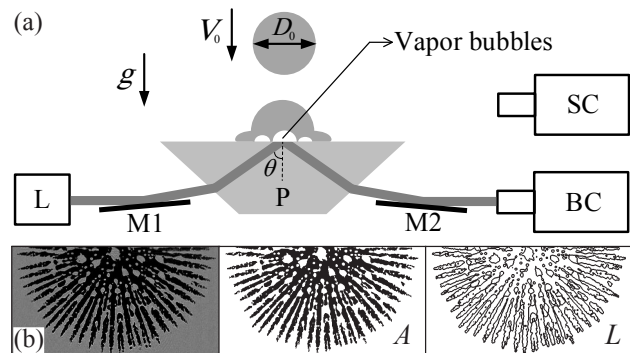


**Fig. 1** (a) Schematic of the experimental setup (not to scale) used to study the impact of droplets on a heated surface. Ethanol droplets of initially uniform diameter  $D_0$  and velocity  $V_0$  fall on the upper surface of a glass prism P that can be heated up to  $350^\circ\text{C}$ . A camera SC is used to measure  $D_0$ ,  $V_0$  and record the impact from the side. A laser beam (640nm in wavelength) emitted from a diode laser and expanded to diameter  $\approx 10\text{mm}$  is directed to a prism using a mirror M1. The beam's incident angle  $\theta$  at the prism's upper surface is adjusted so that the TIR condition is satisfied on the glass-air interface but not on the glass-liquid interface. The reflected beam is directed to a camera BC using a mirror M2. (b) From left to right: Snapshot of a wetted pattern recorded by the TIR method (the wetted area is dark while the dry area is bright). Binary image used to extract the area  $A$  of the wetted pattern. Binary image of the three-phase contact line used to obtain the total length  $L$  of the contact line.

layer generated spontaneously upon impact. Theoretical analysis and modeling<sup>9,12,13</sup> of the heat flux within the contact boiling regime crucially depends on, and is inseparable from, the wetted area. However, quantitative measurements of this quantity have been hindered by several challenges including the very fast dynamics of the impact and nucleating bubbles at the solid-liquid interface, as well as the difficulty in optically distinguishing wetted and dry areas underneath the impacting droplet: the dry areas are covered by an air-vapor layer that is typically only a few micrometers thick<sup>6</sup>. These challenges also prevent an accurate determination of the Leidenfrost transition, as the categorization of impacts in the Leidenfrost regime requires that the liquid does not make contact with the heated surface during the entire impact time.

In this Letter, we investigate previously unexplored boil-

<sup>a</sup> School of Mechanical & Aerospace Engineering, Nanyang Technological University, 50 Nanyang Avenue, 639798, Singapore.

<sup>b</sup> Institute of Materials Research and Engineering, A\*STAR, 3 Research Link, 117602, Singapore.

<sup>c</sup> Physics of Fluids, University of Twente, P.O. Box 217, 7500 AE Enschede, The Netherlands.

\* Email: ttran@ntu.edu.sg

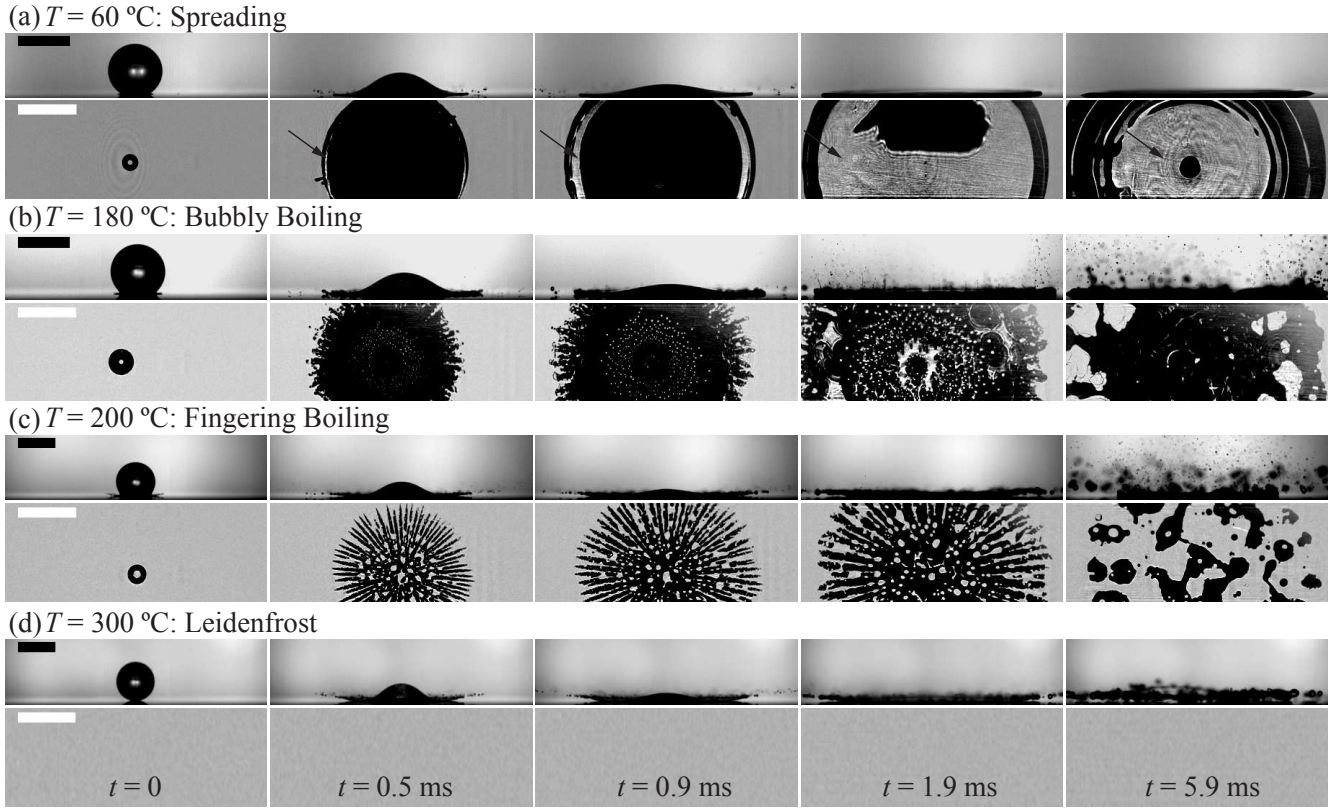


**Fig. 2** Series of the side- and bottom-view snapshots obtained from experiments with different surface temperatures and a fixed  $We = 481$  ( $V_0 = 2.58 \text{ m} \cdot \text{s}^{-1}$ ). Snapshots in the same column are taken at the same time after the impact time ( $t = 0$  is taken at the first frame that a wetted area could be detected). In cases in which the liquid wets the surface and creates a thin, relatively flat film, reflected light from the glass-liquid and the liquid-air interfaces may cause interference patterns, which appear in the TIR recordings as gray areas with dark and bright fringes (see arrows in (a)). It is possible to differentiate these wetted areas from the dry ones based on the presence of fringes. All the inset bars indicate a length scale of 2 mm.

ing behaviors during impact of droplets on superheated surfaces, with an emphasis on the contact boiling regime. In this regime, we measure the absolute area of wetted patterns in a wide range of surface temperature and kinetic energy of the impacting droplets. We also explore and analyze for the first time the striking formation of finger-like patterns that occur during transition to the Leidenfrost regime (illustrated in Fig. 1(b)).

In our experiments, droplets were generated by dispensing liquid out of a flat-tipped needle at a small rate - a droplet formed at the needle's tip falls as soon as the gravitational force overcomes the surface tension force that hangs it. The working liquid was ethanol with density  $\rho = 789 \text{ kg} \cdot \text{m}^{-3}$ , surface tension  $\sigma = 22.4 \times 10^{-3} \text{ N} \cdot \text{m}^{-1}$ , and viscosity  $\nu = 1.4 \times 10^{-6} \text{ m}^2 \cdot \text{s}^{-1}$  (specified at room temperature). The generated droplets had a uniform diameter ( $D_0 = 2 \pm 0.01 \text{ mm}$ ) and fell on a glass prism with a variable velocity ( $0.34 \text{ m} \cdot \text{s}^{-1} \leq V_0 \leq 2.86 \text{ m} \cdot \text{s}^{-1}$ ) depending on the needle's height. The resulting Weber number  $We = \rho V_0^2 D_0 / \sigma$  is independent of  $T$  and spans almost two decades between 8 and 600. The prism was

made of N-BK7 glass (Thorlabs Inc.) with an average surface roughness  $\approx 10 \text{ nm}$  and was placed in a aluminium holder embedded with two cartridge heaters. As a result, the temperature of the prism's upper surface measured by a K-type surface probe (TME Ltd.) can reach up to  $350^\circ \text{C}$ .

In order to obtain the absolute wetted area of the glass surface during droplet impact, we recorded the bottom view of the impact using the Total Internal Reflection (TIR) method<sup>14–17</sup>. We directed an expanded laser beam (diameter 10 mm) to a side surface of the prism so that the refracted beam in the glass medium made an incident angle  $\theta$  to the prism's upper surface. The incident angle was adjusted so that  $\theta_{ga} < \theta < \theta_{ge}$ , where  $\theta_{ga} \approx 42^\circ$  and  $\theta_{ge} \approx 62^\circ$  respectively were the critical angles for total internal reflection at the glass-air and the glass-ethanol interfaces. With this arrangement (see Fig. 1(a)), a beam incident on a dry area of the upper surface was totally reflected back to the glass medium and was directed to a high-speed camera (SA-X2, Photron Inc.), whereas a beam incident on a wetted area refracted into the liquid medium; the dry area then appeared bright and the wetted one dark in

the recorded images (see Fig. 1(b)). We note that in several cases in which the liquid wets the surface and creates a thin, relatively flat film, interference patterns caused by reflected light from the glass-liquid and the liquid-air interfaces may appear in the TIR recordings as gray areas with dark and bright fringes (see arrows in Fig. 2(a)). These wetted areas can still be differentiated from the dry ones based on the presence of fringes. The sensitivity of the TIR method is extremely high: it is capable of distinguishing a dry area from a wetted one as long as the distance between the glass and the liquid is larger than the evanescent wave's thickness  $d = (\lambda/4\pi)(n_g^2 \sin^2 \theta^2 - n_a^2)^{-1/2} \approx 86 \text{ nm}$ <sup>14</sup>, where  $\lambda = 640 \text{ nm}$  is the wavelength of the laser,  $n_a = 1$  and  $n_g = 1.515$  are respectively the refractive indices of air and glass.

We use the side- and the bottom-view (TIR) cameras to observe impacting droplets at different temperatures and Weber numbers. In figure 2, we show four series of snapshots to exemplify typical boiling behaviors at different surface temperatures ( $T = 60^\circ\text{C}$ ,  $180^\circ\text{C}$ ,  $200^\circ\text{C}$ ,  $300^\circ\text{C}$ ) and a fixed Weber number ( $We = 481$ ); each one corresponds to a boiling regime shown in Fig. 3. In the *spreading regime* in which  $T$  is relatively low, an impacting droplet spreads on the surface without any noticeable boiling effect, i.e., no vapor bubbles are observed during the spreading time (see Fig. 2(a)). This regime corresponds to the region of blue squares in Fig. 3. In the *“bubbly boiling” regime* in which the temperature is higher, the TIR recordings show tiny dry areas caused by nucleating vapor bubbles on the glass surface (see Fig. 2(b) at  $t = 0.9 \text{ ms}$ ). Subsequently, these dry areas may either disappear due to detachment of bubbles from the surface or merge with neighboring ones to create larger dry patches. The density of bubble nucleation is observed to grow with  $T$ , consistent with previous studies of nucleate pool boiling<sup>18</sup>. This relation between the nucleation density and  $T$  has also been used in theoretical modeling of the transition to the *Leidenfrost regime*. That is, nucleate boiling at the solid-liquid interface is the mechanism for diminishing the wetted area and the eventual formation of the vapor layer<sup>9,12,19</sup>. In other words, a prediction can be made that the bubbly boiling regime directly transitions to the Leidenfrost regime without any intermediate boiling behavior.

However, as  $T$  is further increased above the range of the bubbly boiling regime, the TIR recordings reveal a striking wetting pattern that is markedly different from those resulted from nucleate boiling and in stark contrast to the prediction for that regime: after the liquid makes contact with the surface, the wetted pattern quickly evolves to consist mainly of two parts: the *“fingering”* one that keeps advancing outwards, and the *“bubbly”* boiling one at the center (see Fig. 2(c) at  $t = 0.5 \text{ ms}$ ). Note that this fingering pattern can also be observed for other liquids such as acetone, isopropanol, Novec 7000 engineering fluids, although the data presented here were obtained using ethanol only. In the phase diagram in Fig. 3,

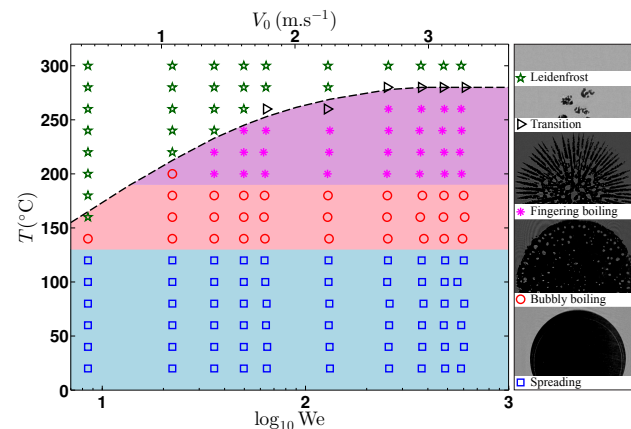


**Fig. 3** (color online) Phase diagram showing four major boiling regimes: spreading (blue squares), bubbly boiling (red circles), fingering boiling (purple asterisks), Leidenfrost (green stars). Several points with transitional behaviors (right triangles) were observed between the Leidenfrost and the fingering boiling regimes: the wetting patterns only appear for a very short time ( $\approx 1 \text{ ms}$ ) and do not have the “fingering” shapes. The dashed line indicates the transition between the fingering boiling and the Leidenfrost regimes. The Weber number was varied by changing  $V_0$  while keeping the droplet diameter fixed ( $D_0 = 2 \pm 0.01 \text{ mm}$ ).

we show the *“fingering boiling” regime* in which the pattern can be observed. The dynamics of the fingering patterns vary with  $T$  and  $We$ . The delay time of the fingering patterns, measured from the frame in which wetting is first observed ( $t = 0$ ), to the one in which the fingering pattern first appears, decreases with increasing  $T$  and  $We$ . The number of fingers also depends significantly on both  $T$  and  $We$  (see Fig. 5). In the *Leidenfrost regime*, the liquid is completely separated from the surface. This can be seen in the TIR recordings (see Fig. 2(d)), i.e., no contact was detected during the impact.

Qualitatively, the different boiling regimes revealed by the TIR method show a much richer dynamics of the spreading liquid and the generated vapor. While the traditional picture of the transition to the Leidenfrost regime only distinguishes between the contact boiling and the non-contact boiling behaviors<sup>6</sup>, the newly-discovered regimes, in particular the fingering boiling regime, show that the transition to the complete non-contact behavior goes through several different stages. Each transitional stage corresponds to a boiling regime and is characterized by a distinct hydrodynamic behavior of the liquid and vapor phases. This insight requires a reconsideration of the Leidenfrost transition. When the vapor generation is excessive, there exists channels created on the surface that allow transport of vapor generated in the center and along three-phase contact lines to the rim of the spreading droplet. Thus, the conductive heat transfer may not be the dominant mode as it is in the bubble boiling regime and transport of vapor is a crucial process in considering the transition to the Leidenfrost

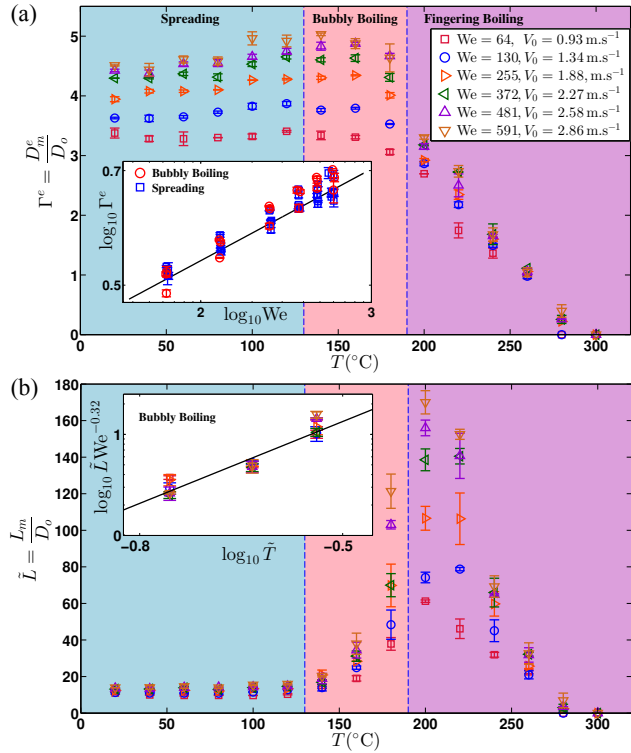


**Fig. 4** (color online) (a) Equivalent spreading factor  $\Gamma^e = D_m^e/D_0$  vs. surface temperature  $T$  for different  $We$ . Inset: log-log plot of  $\Gamma^e$  vs.  $We$  for impacts in the spreading and bubbly boiling regimes. The solid line represents the best fit for the experimental data:  $\Gamma^e \sim We^{0.16}$ . (b) Maximum length of the contact line normalized by the droplet diameter  $\tilde{L} = L_m/D_0$  vs.  $T$  for different  $We$ . Inset: log-log plot of  $\tilde{L}We^{-0.32}$  vs. the normalized superheat  $\tilde{T}$  for different  $We$ . The solid line represents the scaling relationship:  $\tilde{L}We^{-0.32} \sim \tilde{T}^{2.7}$ .

regime.

To quantitatively examine the transitions between different regimes, we measure the wetted area  $A$  during impact (see Fig. 1(b)) as a function of time and extract the maximum value  $A_m$  for each impact experiment. We then define an equivalent maximum diameter based on  $A_m$  as  $D_m^e = \sqrt{4A_m/\pi}$ , which enables comparisons with the apparent maximum spreading  $D_m$  of impacting droplets on unheated surfaces. In figure 4(a), we plot the equivalent spreading factor  $\Gamma^e = D_m^e/D_0$  as a function of  $T$  for different  $We$ . In the spreading regime,  $\Gamma^e$  slightly increases with  $T$  for a fixed Weber number, due to a reduction in the liquid's surface tension. As the impacts enter the bubbly boiling regime,  $\Gamma^e$  starts to decrease gradually because higher  $T$  causes more bubble nucleations and therefore a reduction in the wetted area. However, at any fixed  $We$ , the deviation of  $\Gamma^e$  caused by variation in  $T$  in these two regimes is less than 20% and can be considered insignificant. Therefore, the dependence of  $\Gamma^e$  on  $We$  can be approximated by a single power law  $\Gamma^e \sim We^\alpha$ , where  $\alpha \approx 0.16$  (see inset of Fig. 4(a)).

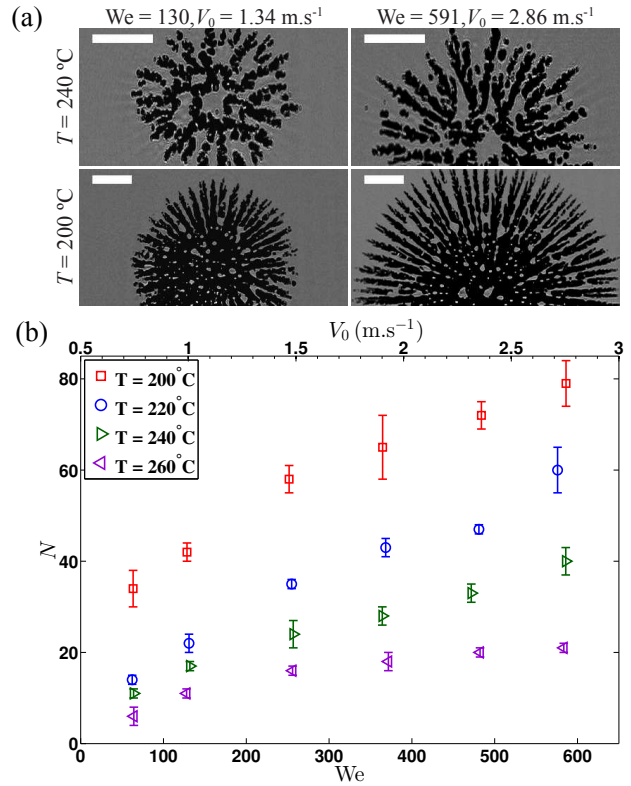


**Fig. 5** (color online) (a) Snapshots of the fingering patterns taken at different  $We$  and  $T$ . All the snapshots were at 0.9ms after the first frame in which wetting is detected. All the inset bars indicate a length scale of 1 mm. (b) Time-averaged number of fingers  $N$  in the fingering boiling regime versus  $We$  for different  $T$ . Note that  $We$  was varied by changing  $V_0$  while keeping the droplet diameter fixed ( $D_0 = 2 \pm 0.01$  mm).

Note that this exponent is not representative of the *apparent* spreading diameter under the liquid, but the one resulted from the *absolute* wetted area. As a comparison, for the impacts of droplets on unheated superhydrophobic surfaces where the spreading liquid is lubricated by an air layer, the scaling exponent is  $\alpha = 0.25$ <sup>20,21</sup>, or for impacts on Leidenfrost surfaces where the vapor provided an extra driving mechanism for the spreading liquid,  $\alpha = 0.3$ <sup>6,22</sup>.

The effect of boiling can be further assessed by examining the total length  $L$  of the three phase contact line of the wetted pattern (see Fig. 1b). For each impact experiment, we can extract  $L$  as a function of time and determine the maximum value  $L_m$ . In figure 4(b) we show a plot of the normalized length contact line  $\tilde{L} = L_m/D_0$  versus  $T$  for different  $We$ . The plot clearly shows that the absence of vapor bubbles in the spreading regime results in a constant  $\tilde{L}$ , whereas bubble nucleation in the bubbly boiling regime causes an abrupt increase of  $\tilde{L}$ . To elucidate the process responsible for the increase in  $\tilde{L}$  in the bubbly boiling regime, we deduce a scaling relationship between  $\tilde{L}$  and  $T$  as follows. If we denote  $N_b$

the density of bubble nucleation, the total number of bubbles scales as  $N_b D_m^e$ . This gives the total length of the contact line  $\sim N_b D_m^e l_b$ , where  $l_b$  is the typical size of vapor bubbles. Thus  $\tilde{L} = L_m/D_0 \sim N_b D_m^e l_b/D_0$ . Here  $N_b$  can be related to the normalized superheat  $\tilde{T} = (T - T_b)/T_b$ , with  $T_b$  the boiling temperature, using a generally accepted scaling relation resulted from nucleate boiling theory:  $N_b \sim \tilde{T}^p$ , where  $p$  is an empirically determined coefficient<sup>18</sup>. The dependence of  $l_b$  on  $T$  is considered weak<sup>18</sup> and can be neglected. Similarly, since  $D_m^e$  was shown insensitive to changes in  $T$  (in both the spreading and the bubbly boiling regimes), we consider it as a function of  $We$  only:  $D_m^e \sim D_0 We^{0.16}$ . Thus, we obtain  $\tilde{L} \sim We^{0.32} \tilde{T}^p$ . In the inset of Fig. 4, we show a log-log plot of  $\tilde{L} We^{-0.32}$  versus  $\tilde{T}$  for different  $We$ . A best fit of the data gives  $p = 2.7 \pm 0.9$ , which is within and at the lower end of the reported range  $2 < p < 6$ <sup>18,23–25</sup>. We note here that the large error of the estimation of  $p$  in our experiments is due to the limited range of  $\tilde{T}$ . The wide range of the reported values of  $p$  may originate from many attributing factors including the material of the surface and how it is prepared, but it is generally accepted that  $p$  is smaller for smoother surfaces<sup>18,26</sup>. Together with the experimental observation, this strongly suggests that the dominant thermal process in the bubbly boiling regime is nucleate boiling.

The transition between the bubbly boiling and the fingering boiling regimes marks a distinctive change in the dependence of  $\Gamma^e$  on  $T$  and  $We$  (Fig. 4(a)):  $\Gamma^e$  becomes insensitive to changes in  $We$  but decreases with increasing  $T$  and eventually diminishes at the Leidenfrost temperature. It is also remarkable that exactly at this transition,  $\tilde{L}$  starts decreasing with increasing  $T$  (Fig. 4(b)). This implies that the dominant thermal process is no longer nucleate boiling and the heat transfer rate from the surface to the liquid starts decreasing and eventually minimizes at the Leidenfrost transition. Thus, the continuous reduction of  $\Gamma^e$  and  $\tilde{L}$  in the fingering boiling regime, which spans a significant temperature range, quantitatively shows that the Leidenfrost transition is continuous and should be considered with mass transport of vapor taken into account.

Let us now discuss the wetted patterns observed in the fingering boiling regime. In figure 5 (a), we shows several snapshots of the fingering patterns at different  $We$  and  $T$ . All the snapshots were taken at the same time (0.9 ms) after impact. Although the fingering patterns can only be observed within a limited range of temperature ( $200^\circ\text{C} \leq T \leq 260^\circ\text{C}$ ), the geometry of these patterns change substantially with temperature. At lower  $T$  ( $T = 200^\circ\text{C}$ ), the fingers appear more slender with larger quantity, whereas at higher  $T$  ( $T = 260^\circ\text{C}$ ), they are more fragmented and have larger width with smaller quantity. Varying the Weber number from 130 to 591 does not seem to significantly change the geometry of these patterns. Note that after the liquid film is completely flattened and sub-

sequently ruptured, the liquid fragments may also form patterns with fingering geometry, which can be observed using top-view recordings<sup>27</sup>. The difference between the ones in our present study and these patterns is that the former ones occur at the very early stage of the impact; during this stage, the liquid at the center still has the shape of a spherical cap and remains intact, while the later one occur at a later stage due to fragmentation of the liquid film. To quantitatively characterize this behavioral change of the patterns, we count the number of “fingers” for each impact experiment as a function of time and take the time-averaged number  $N$ . In figure 5(b), we show a plot of  $N$  versus  $We$  for different  $T$ . It can be seen that  $N$  increases with  $We$  but decreases with  $T$ . Although it is not clear to us what causes this dependence of  $N$  on  $We$  and  $T$ , we conjecture that the formation of these patterns is related to the instability of the vapor flow as it is squeezed out from the gap between the droplet and the solid surface. Therefore this phenomenon calls for more thorough experimental and theoretical investigations at the onset of impact.

In summary, we have presented measurements of the absolute wetted area during the boiling and spreading processes of droplets impacting on heated surfaces. In particular, we have shown that the boiling behaviors of impacting droplets on heated surfaces can be mainly divided into four major regimes: the spreading regime in which the heating effect is negligible, the bubbly boiling regime in which nucleate boiling is activated at the solid-liquid interface, the fingering boiling regime whose characteristics include (i) a gradual decrease in the wetted area with increasing temperature, (ii) an independence of the wetted area from the Weber number, and (iii) vapor transport between the “fingers” of the wetted patterns, and finally the Leidenfrost regime. Measurements of the wetted area in these boiling regimes indicate that the transition to the Leidenfrost regime is continuous with respect to the wetted area and an understanding of its physical mechanism requires incorporation of vapor transport under the liquid, which vapor flow is closely related to the formation of the fingering wetted pattern. Since the heat transferred to the liquid is mostly through the contact area, the continuous reduction of the contact area with surface temperature, together with the dynamical characteristics of the three contact boiling regimes, may serve as building blocks for modeling of the heat transfer between the heated surface and the impacting droplet. A preliminary analysis of the the patterns indicates a dependence of the number of fingers on the Weber number and surface temperature, but further theoretical and experimental work is needed to understand the formation of these patterns. We anticipate that these quantitative measurements of the wetted area will provide new insights into obtaining a complete understanding of the Leidenfrost transition.

We thank C.D. Ohl, M.S.M Saifullah, and P. Chakraborty for helpful discussions. This study was financially supported

---

by the Nanyang Technological University. M. Khavari is supported by SINGA scholarship (A\*STAR). We also thankfully acknowledge support by an ERC-Advanced Grant.

## References

- 1 M. Rein, *Drop-surface interactions*, Springer Verlag Wien, 2002, vol. 428.
- 2 A. Moreira, A. Moita and M. Panão, *Prog. Energy Combust. Sci.*, 2010, **36**, 554–580.
- 3 F. Akao, K. Araki, S. Mori and A. Moriyama, *Trans. Iron Steel Inst. Jpn.*, 1980, **20**, 737–743.
- 4 K. Takeuchi, J. Senda and K. Yamada, Proceedings of the ASME-JSME Thermal Engineering Joint Conference, 1983, pp. 165–172.
- 5 A. Wang, C. Lin and C. Chen, *Phys. Fluids*, 2000, **12**, 1622.
- 6 T. Tran, H. J. Staat, A. Prosperetti, C. Sun and D. Lohse, *Phys. Rev. Lett.*, 2012, **108**, 036101.
- 7 L. Wachters and N. Westerling, *Chem. Eng. Sci.*, 1966, **21**, 1047–1056.
- 8 J. Bernardin, C. Stebbins and I. Mudawar, *Int. J. Heat Mass Transfer*, 1997, **40**, 247–267.
- 9 J. Bernardin and I. Mudawar, *J. Heat Transfer*, 2004, **126**, 272.
- 10 J. Leidenfrost, *Duisburg*, 1756.
- 11 D. Quéré, *Annu. Rev. Fluid Mech.*, 2013, **45**, 197–215.
- 12 J. Bernardin and I. Mudawar, *J. Heat Transfer*, 1999, **121**, 894.
- 13 P. Pournaderi and A. Pischevar, *Heat Mass Transfer*, 2012, **48**, 1525–1538.
- 14 E. Hecht, *Optics*, Addison Wesley, 2002.
- 15 P. Huang, J. S. Guasto and K. S. Breuer, *J. Fluid Mech.*, 2006, **566**, 447–464.
- 16 J. M. Kolinski, S. M. Rubinstein, S. Mandre, M. P. Brenner, D. A. Weitz and L. Mahadevan, *Phys. Rev. Lett.*, 2012, **108**, 074503.
- 17 J. M. Kolinski, L. Mahadevan and S. M. Rubinstein, *Phys. Rev. Lett.*, 2014, **112**, 134501.
- 18 V. Dhir, *Annu. Rev. Fluid Mech.*, 1998, **30**, 365–401.
- 19 B. Gottfried, C. Lee and K. Bell, *Int. J. Heat Mass Transfer*, 1966, **9**, 1167–1188.
- 20 C. Clanet, C. Béguin, D. Richard and D. Quéré, *J. Fluid Mech.*, 2004, **517**, 199–208.
- 21 P. Tsai, M. H. Hendrix, R. R. Dijkstra, L. Shui and D. Lohse, *Soft Matter*, 2011, **7**, 11325–11333.
- 22 T. Tran, H. J. Staat, A. Susarrey-Arce, T. C. Foertsch, A. van Houselt, H. J. Gardeniers, A. Prosperetti, D. Lohse and C. Sun, *Soft Matter*, 2013, **9**, 3272–3282.
- 23 C. Wang and V. Dhir, *J. Heat Transfer*, 1993, **115**, 659–669.
- 24 R. Benjamin and A. Balakrishnan, *Exp. Therm Fluid Sci.*, 1997, **15**, 32–42.
- 25 S. Cheung, S. Vahaji, G. Yeoh and J. Tu, *Int. J. Heat Mass Transfer*, 2014, **75**, 736–753.
- 26 K. Cornwell and E. Brown, 6th Int. Heat Transfer Conference. Toronto, Canada, 1978.
- 27 S. Manzello and J. Yang, *Int. J. Heat Mass Transfer*, 2002, **45**, 3961–3971.